

1-21-1991

Imaging of Magnetic Microstructures at Surfaces: The Scanning Electron Microscope with Spin Polarization Analysis

H. P. Oepen

Institut für Grenzflächenforschung und Vakuumphysik Forschungszentrum Jülich

J. Kirschner

Institut für Experimentalphysik

Follow this and additional works at: <https://digitalcommons.usu.edu/microscopy>



Part of the [Biology Commons](#)

Recommended Citation

Oepen, H. P. and Kirschner, J. (1991) "Imaging of Magnetic Microstructures at Surfaces: The Scanning Electron Microscope with Spin Polarization Analysis," *Scanning Microscopy*: Vol. 5 : No. 1 , Article 1.

Available at: <https://digitalcommons.usu.edu/microscopy/vol5/iss1/1>

This Article is brought to you for free and open access by the Western Dairy Center at DigitalCommons@USU. It has been accepted for inclusion in Scanning Microscopy by an authorized administrator of DigitalCommons@USU. For more information, please contact digitalcommons@usu.edu.



IMAGING OF MAGNETIC MICROSTRUCTURES AT SURFACES:
THE SCANNING ELECTRON MICROSCOPE WITH SPIN POLARIZATION ANALYSIS

H.P. Oepen*

Institut für Grenzflächenforschung und Vakuumphysik
Forschungszentrum Jülich, Postfach 1913, D-5170 Jülich, West Germany

J. Kirschner

Institut für Experimentalphysik, Freie Universität Berlin
Arnimallee 14, D-1000 Berlin 33, West Germany

(Received for publication April 15, 1990, and in revised form January 21, 1991)

Abstract

The scanning electron microscope with spin polarization analysis of secondary electrons has been proven to be a powerful tool for studying magnetic microstructures. Secondary electrons created at the surface of a ferromagnet are spin-polarized and contain information about the sample magnetization and its orientation. The combination of a spin polarization analyzer with a scanning electron microscope yields a unique apparatus for probing magnetic properties on a very small lateral scale. The magnetic resolution of < 40 nm is demonstrated. This type of microscope provides high magnetic contrast, while the surface morphology is strongly or even totally suppressed. The capability of studying magnetic properties of semi-infinite samples as well as in ultrathin films is demonstrated with a Fe(100) single crystal, video tape, CoCr perpendicular recording medium and ultrathin cobalt films.

KEY WORDS: Spin polarization, magnetic microstructure, storage media, surface and thin films magnetism.

*Address for correspondence:
H.P. Oepen, IGV, KFA Forschungszentrum Jülich,
Postfach 1913, D-5170 Jülich, West Germany
Phone No.: (49) 2461-61-6516

Introduction

Magnetism and its manifestation is one of the most complex fields of solid state physics. One of the reasons for its extraordinary position is the fact that many macroscopic properties of magnets depend on mesoscopic quantities i.e. the magnetic domains and their equilibrium configuration. Domain configurations can only be calculated in ideal cases. In general, they are very complex and can be determined only by observation. The experimental study of the micro-magnetic structure, e.g. the shape and size of domains, the direction of magnetization in each domain, or the change of domain configurations in the reversal process, has given an impetus to the understanding of many properties of magnets. Still there are, however, a number of unresolved questions demanding new techniques for studying the magnetic microstructure with high spatial resolution. A major goal of magnetic data storage technology is to increase the storage density via miniaturizing the lateral size of the smallest information stored, the bit. In miniaturizing the bits their magnetic boundary quality, i.e. their sharpness and smoothness, as well as the homogeneity of magnetization of the bits gain more and more importance for the noise in the reading process. For optimizing the medium quality with respect to such questions there is again a strong need for analyzing techniques with high spatial resolution.

Recently, investigations of ultrathin ferromagnetic films, with thicknesses of a few monolayers, have become feasible, as the techniques of preparation and growth have been improved. Monolayer films open the opportunity to study the influence of dimensionality and the influence of surfaces and interfaces on magnetism. The requirements on any experimental technique are high, since a high sensitivity for samples of vanishing thickness is essential, besides high resolution. A powerful technique, promising high spatial resolution and high surface sensitivity as well, had been proposed about a decade ago (DiStefano, 1978; Unguris et al., 1982; Kirschner, 1984). Soon after these suggestions this new domain observation method was actually realized (Koike and Hayakawa, 1984a; Unguris et al., 1985). This technique uses the highly focused unpolarized electron

Table 1: List of symbols.

A	scattering asymmetry
C	image contrast
e^-	elementary charge
F	figure of merit
I_p	probe current
M_s	saturation magnetization
$N_{A,B}$	number of electrons scattered into opposite channels
N_o	number of electrons entering the polarization detector
N_s	noise
P	spin polarization
S	polarization sensitivity
t	measuring time
T	transmission of the detector electron optics
Y	secondary electron yield
δS	signal difference from different magnetic domains
η	scattering efficiency

beam of a scanning electron microscope (SEM) to generate secondary electrons, the polarization of which is subsequently measured to obtain the magnetic information. Some of the advantages of this technique have been demonstrated in the last few years, e.g. high magnetic contrast nearly independent of surface morphology (Koike and Hayakawa, 1984b), or high spatial resolution (Oepen and Kirschner, 1989).

Compared to all the other methods of domain observation the scanning electron microscope with spin polarization analysis of the secondary electrons provides the magnetization vector orientation directly, which is one of the most important advantages of this technique. With regard to the lateral resolution it is superior to many conventional methods, such as Bitter techniques (Bitter, 1931; Hámos and Thiessen, 1931), Kerr- and Faraday-microscopes (Rave et al., 1987), (resolution $> 0.2 \mu\text{m}$), and the SEM methods with type I and II contrast (Newbury et al., 1986) (resolution $> 1 \mu\text{m}$). The actually achieved lateral magnetic resolution is better than 40 nm (Oepen and Kirschner, 1988). Magnetic force microscopy also holds great promise, though its detailed interpretation may pose serious question. The established techniques attaining higher resolution, equal or less than 10 nm, like Lorentz microscopy (Jacubovics, 1973; Chapman and Morrison, 1983) and electron holography (Tonomura, 1983), are limited to thin samples, as they work in transmission only. Therefore the samples have to be thinned for investigation, which may in turn affect their magnetic properties. The contrast obtained, depends on the Lorentz force due to the magnetic flux along the

whole electron path, thus measuring an integrated quantity not only through the sample but also outside it. The scanning electron microscope with spin polarization analysis works in the emission mode, thus being capable of investigating semi-infinite samples as well as thin and ultrathin films.

Of course, each technique has its specific advantages and drawbacks and it depends very much on the particular application, which one is the best to attack a given problem. Since a complete overview over different techniques must lie outside the scope of this paper, we line out the particular advantages and limitations of this type of microscope. Some illustrative examples are given for a number of different applications. After briefly discussing the underlying physics of the technique, we concentrate on the apparatus built up at the KFA (Oepen and Kirschner, 1988), although most of the results and considerations are also valid and applicable to other microscopes with spin polarization analysis.

Basic Effects

Secondary electron spin polarization

In 1976, Chobrok and Hofmann (Chobrok and Hofmann, 1976) found that the secondary electrons ejected from a ferromagnet are spin-polarized. Little attention was paid to this discovery until 1982, when the first systematic energy resolved studies on the secondary electron spin polarization from ferromagnets were carried out (Unguris et al., 1982; Kisker et al., 1982). Since then this effect has been extensively studied by many groups. It has been found, that the polarization of the secondaries exhibits a pronounced dependence on their energy, in fact not depending on the kind of particles they are created by (Kirschner et al., 1988). A typical result of an angle- and energy resolved study is shown in Fig. 1. The upper curve shows the intensity - the lower one the polarization distribution of the secondary electrons from a Fe(110) single crystal surface, excited by electrons of 2 keV energy. The highest polarization is found for the electrons with nearly zero kinetic energy (see Fig. 1), just at the peak of the intensity distribution. With increasing secondary electron energy the polarization decreases smoothly and ends up at energies above 20 eV with a value of about 28 %, approximately the net spin polarization of the valence band electrons of iron. Some fine structure is also seen in the polarization distribution, which we do not discuss here. For more details the reader is referred to Kirschner (Kirschner, 1988). The most exciting feature of the secondary electron polarization is its maximum value of about 50 %, which is nearly twice the value of the valence band electron spin polarization. The reason for this enhancement is commonly believed, though still a subject of current debate and studies, to be a consequence of the cascade process of secondary electron creation and the inelastic processes involved. The energy loss process via electron-electron interaction in the cascade is determined by the different density of states

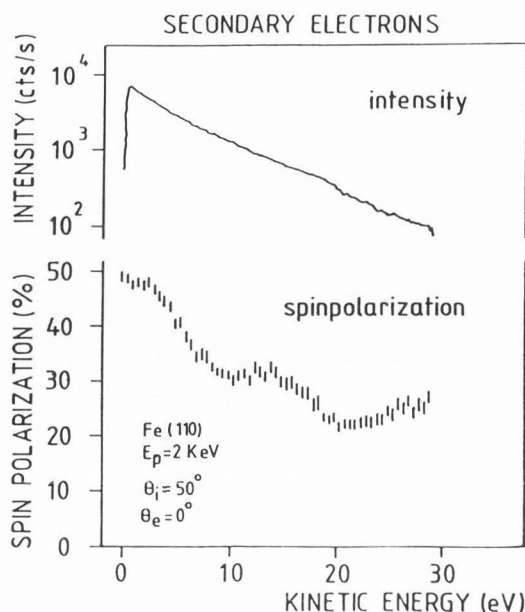


Figure 1. Logarithmic intensity and spin polarization distributions of secondary electrons emitted normally from clean Fe(110) as a function of their kinetic energy. The primary energy is 2 KeV and the angle of incidence is about 50° .

below and above the Fermi energy for majority and minority spin electrons. Thus preferentially, majority spin electrons are excited, while a higher possibility exists for minority spin electrons to be inelastically scattered. The possibility of the latter process rises with decreasing energy of the electrons to be scattered. At very low energies, around threshold, the electrons can be inelastically scattered into states near the Fermi level only. Above the Fermi level, however, there is a strong imbalance of unoccupied minority and majority states. Due to the considerably higher density of minority states, preferentially minority electrons are scattered inelastically. This leads to a strong suppression of the minority spin electrons at low energies, being responsible for the enhanced majority-type polarization of the ejected electrons. The decrease of the polarization (Fig. 1) shows that the filtering effect becomes weaker with increasing secondary electron energy. At about 20 eV the polarization is roughly equal to the net spin polarization of the valence band electrons.

This is the effect behind the very advantageous combination of high polarization and high intensity at low secondary electron energy. This circumstance is an essential condition for obtaining high contrast in a scanning electron microscope with polarization analysis, as will be discussed in detail below. Some other features of the cascade induced secondary electron polarization should be mentioned. Firstly, a direct correlation between the polarization vector and magnetization orientation was found. It is actually the magnetization direction which de-

termines the orientation of the spin polarization vector (Kirschner and Suga, 1987), i.e. the polarization vector lies antiparallel to the magnetization vector. This opens the opportunity to determine the magnetization orientation directly via the polarization vector determination. In the scanning electron microscope with polarization analysis, it is actually the polarization magnitude and orientation that gives the signal used to obtain the magnetic image. Secondly, it was found empirically that the polarization of the secondary electrons scales roughly with the saturation magnetization (M_s) of the material. From that, one can estimate the polarization (P), which is to be expected for different ferromagnetic materials. For example in the case of cobalt the polarization near zero kinetic energy is about

$$P(\text{Co}) = \frac{M_s(\text{Co})}{M_s(\text{Fe})} \cdot P(\text{Fe}) = 40\% \quad (1)$$

Finally it is important to note that in an angle integrated experiment the intensity maximum shifts to somewhat higher energies (to about 2 eV) (Seiler, 1983), due to emission cone effects. The spin polarization is only slightly reduced at that energy.

The depth of information

A considerable body of information on the escape depth of secondary electrons has been accumulated, mainly in connection with scanning electron microscopy. According to Seiler (Seiler, 1983) the escape depth ranges from 0.5 to 1.5 nm for metals. The smallest escape depths are found for d-band metals with half filled d-shells (Makharov and Petrov, 1981). These considerations are valid in general without any reference to the spin polarization. Recalling from above that the largest polarization value is found at very low energies it is evident that in both applications electrons of the same energy are used. Thus the depth of information should be similar. Experimentally, the magnetic probing depth in spin-polarized secondary electron spectroscopy has been studied by Abraham and Hopster (Abraham and Hopster, 1987). They found the escape depth to be about 0.5 nm in excellent agreement with the above values. The same has been found in the investigation of the domain structure of ultrathin ferromagnetic films, which will be discussed later on. Although the probing depths appear to be the same, there are remarkable differences between conventional scanning electron microscopy and the observation of magnetic structures via spin polarization analysis. To form a topographic image it is of minor or even no importance at what depth the secondary electrons are created. The structure is even well observable if the electrons are produced in an overlayer and, indeed, for many applications the samples are coated on purpose. In the scanning electron microscope with spin polarization analysis, however, only the electrons from the ferromagnetic part of the sample are spin-polarized and thus contain the information about the magnetic structure. From that it is evident that for this type of micro-

scope the meaning of the phrase "depth of information" is more restrictive than for conventional topographical microscopy. Any coating or any surface coverage due to residual gas adsorption may suppress all the magnetic signal, while a topographic contrast is preserved. Even very small amounts of contamination may strongly reduce the polarization signal. It has been shown that for iron one monolayer of oxygen reduces the polarization by more than a factor of two (Allenspach et al., 1985). That finding clearly demonstrates the necessity for clean surfaces as an important prerequisite for a successful domain structure observation. To achieve clean surfaces the samples have to be prepared in situ using the traditional surface science cleaning techniques. To keep surfaces clean for a certain amount of time, at least for the time of taking an image, the whole experiment has to be performed under ultra high vacuum conditions. These essential requirements may be a disadvantage for the microscope with polarization analysis for some applications. On the other hand, the small depth of information can be used to advantage. First of all the technique allows the study of surface magnetism, i.e. the magnetic properties of the topmost few layers. Secondly, the technique is unique for studies of ultrathin films. The ferromagnetic properties of such films in the thickness range of some monolayers exhibit highly interesting behaviour due to the transition from three to two dimensional magnetism. Some examples of magnetic microstructures in monolayer films are discussed below.

Scanning Electron Microscope with Spin Polarization Analysis

Spin polarization measurement

Various methods are used to detect the spin polarization of electrons, such as the Mott detector (Kessler, 1985), LEED detector (Kirschner, 1985), absorption current detector (Siegmann et al., 1981), low energy diffuse scattering detector (Unguris et al., 1986). All of them have been used in scanning electron microscopes with spin polarization analysis (Koike and Hayakawa, 1984a; VanZandt et al., 1989; Oepen and Kirschner, 1988; Koike et al., 1988; Unguris et al., 1985). As we use the LEED detector in our microscope, this detector is explained in some detail.

The principle of the LEED detector is explained with reference to Fig. 2. The electrons to be analyzed are focused by an electrostatic lens onto a W(100) single crystal. The intensities (N_A, N_B) of two equivalent diffraction beams, here the (2,0) beams, are measured for the polarization analysis. Due to spin orbit interaction in the scattering process oppositely diffracted beams exhibit different intensities if the incoming electrons are spin-polarized. The measured asymmetry,

$$A = \frac{N_A - N_B}{N_A + N_B}, \quad (2)$$

is proportional to one polarization component. This component is perpendicular to the scatter-

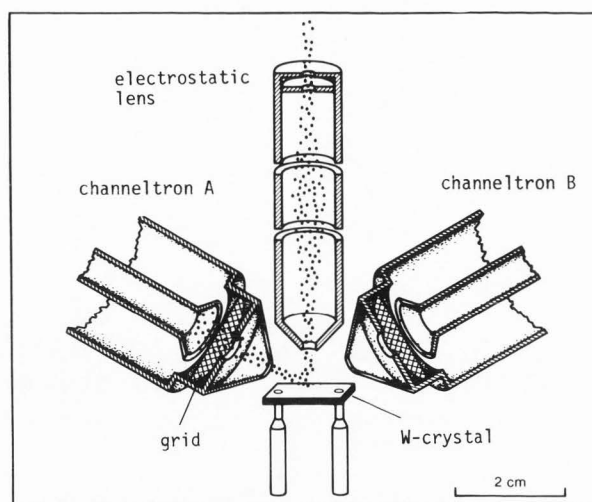


Figure 2. Principle of the spin polarization analysis. The electrons are focussed onto the W(100)-crystal by means of the electrostatic lens. The electron detection units (channeltrons) are positioned in such a way as to accept the diffracted beams of second order. To separate the elastically diffracted electrons from the inelastically scattered one a grid assembly is mounted in front of the channeltrons. To measure the intensities the channeltrons are run in the counting mode yielding a high signal to background ratio. The asymmetry

$$A = \frac{N_A - N_B}{N_A + N_B}$$

is proportional to the polarization component perpendicular to the scattering plane, i.e. the plane of drawing.

ing plane, which is spanned by the incoming and diffracted beams. The polarization is given by

$$P = \frac{1}{S} \cdot A, \quad (3)$$

with S the sensitivity of the detector. S is the asymmetry one would measure with totally polarized electrons. The sensitivity of the LEED detector, using the (2,0) diffraction beams with a scattering energy of 104.5 eV is $S = -0.25$, in our case.

As the W(100)-crystal has fourfold symmetry, there are two additional (2,0) beams, which can also be used for spin polarization detection. With these beams a second polarization component, perpendicular to the former one, can be measured. Fig. 3 shows a top view of the detector with its fourfold symmetrical arrangement of the electron counting facilities, and the W crystal in the center. The two polarization components, which can be measured with that detector, run parallel to the large and short sides of the W-crystal.

A commonly used quantity to characterize the efficiency of spin detectors is the so-called figure of merit

$$F = S^2 \cdot \eta \quad (4)$$

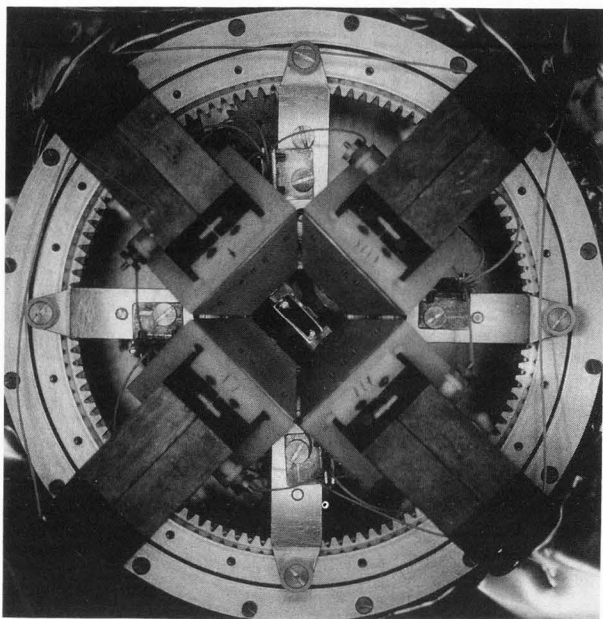


Figure 3. Top view of the LEED spin polarization analyzer. The W(100)-crystal in the centre as well as four multiplier housings are to be seen. The two polarization sensitive axes of the detector are parallel to the crystal edges ($\{100\}$ -directions). The whole assembly is equipped with a ball bearing for rotating the detector as a whole about the crystal surface normal. The diameter of the system is < 150 mm.

$$\text{with } \eta = \frac{N_A + N_B}{N_0} \quad (5)$$

and N_0 the number of electrons entering the detector. For our LEED detector

$$F \approx 1 \cdot 10^{-4}, \quad (6)$$

a value that is similar for all the above listed detector systems. Among detectors of equal figures of merit, however, the one with a large polarization sensitivity S is preferable, since it is less sensitive to instrumental asymmetries. The LEED detector has a good sensitivity and is therefore well applicable also in cases with small magnetic signals (see results: CoCr storage medium).

Principle of domain observation

The principle of domain observation using a scanning electron microscope with spin polarization analysis is shown in Fig. 4. A fine primary electron beam is scanned across the magnetic sample. Secondary electrons are created in a very small spot with lateral dimensions of the order of the primary beam diameter. As mentioned above, the secondary electrons are spin-polarized and their polarization vector points anti-parallel to the magnetization (parallel to the majority spin polarization orientation of the valence band electrons as shown in Fig. 4). Mea-

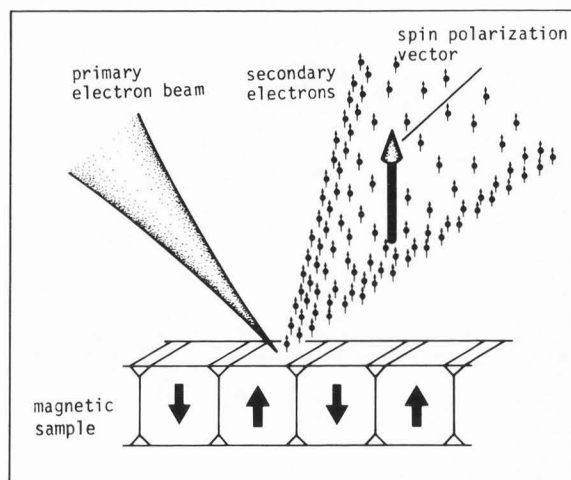


Figure 4. Principle of magnetic structure analysis in a scanning electron microscope with spin polarization analysis. The finely focussed primary beam excites secondary electrons at the surface within a small spot. The spin polarization of these electrons is analyzed and used as a signal for image production.

suring the orientation of the spin polarization thus yields the magnetization orientation at each point, or in other words the magnetization distribution of the sample, i.e. the domain pattern.

A sketch of our experimental set up is shown in Fig. 5. The whole experiment is performed under ultra high vacuum conditions for the reasons mentioned above. The electron microscope column is equipped with a field emission source yielding a spatial resolution of 3 nm at 25 keV. The beam energy can be varied between 300 eV and 25 keV. The base resolution at 500 eV is < 100 nm and < 20 nm at 1 keV.

A specially designed focussing lens picks up the secondary electrons and focusses them into the spin polarization analyzer. The detector arrangement shown allows the determination of the two magnetization components oriented parallel to the sample surface at grazing incidence of the primary beam. Depending on the tilt of the sample, the projection of the component in the paper plane is measured (see Fig. 5). A second detector position, not shown in the sketch, is positioned at an angle of 90° to the former one. This detector allows to measure additionally the third magnetization component, perpendicular to the sample surface. To reach this second spin polarization analyzer the electrons are bent by 90° on passing through an energy analyzer, mounted behind the focussing lens. The two detectors are selected by turning the energy analyzer on and off.

The sample is typically at 45° with respect to the column and the focussing lens. This arrangement has been preferred to obtain a good compromise between a loss of resolution due to the glancing incidence of the primary electrons and a reduction of secondary electron intensity due to a reduction of the accepted secondary

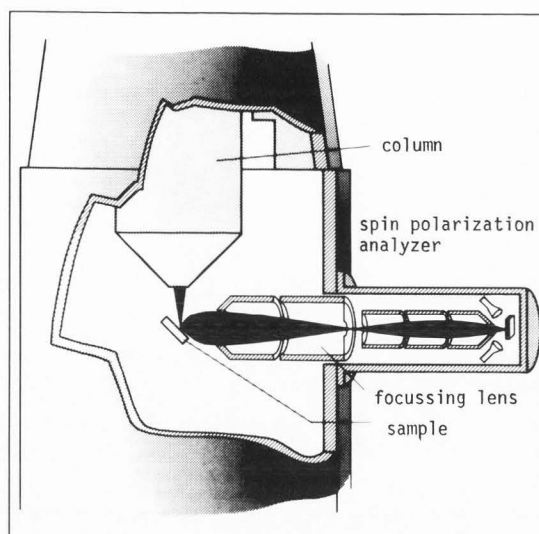


Figure 5. A sketch of the scanning electron microscope with spin polarization analysis of the secondary electrons. The arrangement of the spin analyzer allows to measure two magnetization components within the sample surface. A second detector position is available orthogonal to the one shown. To focus the electrons into this detector an electrostatic deflector is installed behind the focussing lens. By this equipment the electrons are bend by 90° (coming out of the plane of drawing) and enter a second analyzer. This analyzer allows to measure one in-plane magnetization component and the magnetization perpendicular to the sample surface.

electron emission cone. Moreover it is desirable to separate column and optics as much as possible, as the stray magnetic fields from the column may possibly change the polarization orientation of the electron spins via Larmor precession on their way to the detector. To minimize this effect and to maximize the optics acceptance angle, the electrons are accelerated into the focussing lens. No influence of the stray magnetic fields of the column objective lens on the polarization orientation was detected.

Image contrast

What is the magnetic contrast one can obtain with the scanning electron microscope with polarization analysis? For distinguishing two different areas in an image, the ratio

$$C = \frac{\delta S}{N_S} \quad (7)$$

of the signal difference δS from the two areas and the noise N_S should be sufficiently high ($C > 1$) (Koike et al., 1987). That means, if one wants to distinguish between the two oppositely magnetized domains of Fig. 4, it is $\delta S = 2P$. If we assume the predominant noise to be statistical noise, we may write

$$N_S = \frac{1}{\sqrt{F \cdot N_0}} \quad (8)$$

with $F = \eta \cdot S^2$ the figure of merit and N_0 the number of electrons entering the detector (Kessler 1985). Thus we obtain for the contrast

$$C = 2P \cdot \sqrt{F \cdot N_0} \quad (9)$$

N_0 can be expressed by parameters characterizing the various properties of the microscope. N_0 is obviously proportional to the number of primary electrons hitting the sample, which can be expressed as

$$I_{P/e^-} \cdot t \quad (10)$$

with the probe current I_P , the measuring time t and the elementary charge

$$e^- = 1.6 \times 10^{-19} \text{ C.} \quad (11)$$

As each primary electron produces Y secondary electrons and a fraction T of those secondary electrons is transmitted by the electron optics from the sample to the detector, one can write

$$N_0 = T \cdot Y \cdot (I_{P/e^-} \cdot t). \quad (12)$$

Thus one obtains for the contrast

$$C = 2P \cdot \sqrt{F \cdot T \cdot Y \cdot (I_{P/e^-} \cdot t)} \quad (13)$$

We would like to discuss equation (13) in more depth, as it shows the capabilities and limits of this kind of microscopy.

First of all it is interesting to realize the strong dependence of contrast on the spin polarization of the secondary electrons. There is a linear dependence on P whereas all the other quantities show a square root dependence. In other words, a loss of P by a factor f , needs a factor f^2 to be gained by one of the other factors or by the measuring time. Remembering the energy dependence of the secondary electron spin polarization (see Fig. 1), it is obviously favorable and in most cases even necessary to select the very low energy electrons for image formation. Thus an energy dispersive element in the analyzer equipment is most favorable. In our microscope electrons with energies ranging from 0 to 6 eV are used, yielding high polarization and high intensity as well.

A further consequence of the polarization dependence of the contrast is that it also imposes some restrictions on the materials that can be investigated with this technique. If P scales roughly with M we can estimate the contrast one can expect with different materials. With iron we can easily obtain a contrast of ≥ 10 (see examples below) in a very short time of $t \approx 10$ msec/pixel, yielding a total time of ~ 10 minutes to obtain a picture of 250×250 pixels. For a material like Ni ($M_S = 1/3 M_S(\text{Fe})$) one may extrapolate a measuring time of ~ 100 msec/pixel to achieve the same contrast. For materials with much lower saturation magnetization than Ni it is very difficult to obtain the same picture quality in acceptable times. Another consequence of the dependence of the contrast C on the polarization is the requirement of a clean surface, especially with material of

Low saturation magnetization, as the polarization is drastically lowered by small amounts of any contaminants (see above).

The other quantities in formula (13) are more or less related to the experimental set up and the special features of the different components. F , the figure of merit, is the efficiency of the spin analyzer. As mentioned above, its value is of the order of 10^{-4} for all existing kinds of spin polarization detectors, which is extremely small compared to the electron multiplier efficiency (~ 1) used in normal SEM applications. In principle, the figure of merit could be about three orders of magnitude higher, but unfortunately no such device has yet been invented. This particular property of polarization analyzers presently demands the optimizing of all the other parameters at hand.

The transmission T is defined as the ratio of the number of electrons entering the detector to the total number of electrons leaving the sample with energies up to 6 eV. Thus T does not only describe the quality of the electron optics but it also contains the loss of intensity due to the limited acceptance angle and the energy filtering. In fact our measured value for T is mainly determined by the size of the acceptance cone due to the 45° sample tilt. With 0 - 6 eV electrons we find a transmission of 10 % for our experimental geometry.

The secondary electron yield Y depends on the material as well as on the energy of the primary beam. The dependence of the total electron yield and secondary electron spin polarization on the primary electron energy for iron is shown in Fig. 6. As one can see the total electron yield exhibits a pronounced maximum at about 500 eV, whereas the spin polarization saturates at about 1 keV for secondary electrons of 1 eV kinetic energy. Above 1 keV the polarization remains constant. A detailed discussion and interpretation of that result is published elsewhere (Kirschner, 1988). We will focus our attention on its consequences for the optimal working condition of the microscope. From equation (13) it is evident that the product $P^2 Y$ should be a maximum to obtain highest contrast. It turns out that the highest value of the product is to be found at about 1 keV primary energy, when the polarization has reached its maximum value and the total electron yield is still high. From this result, together with the remaining quantity I_p/e^- of formula (13), we may

directly derive the requirements on the electron gun, i.e. the scanning electron microscope column: The column should be able to give high intensity, certainly with high spatial resolution, at low primary energies in the range of 1 keV (to maximize $P^2 \cdot Y \cdot I_p/e^-$). These requirements are best satisfied by scanning electron microscope columns with a field emission source. Such a column is used in our microscope. We may obtain probe currents of about $1 \cdot 10^{-9}$ A at 1 keV with spatial resolution of ≤ 50 nm.

Results

The domain images shown below all consist of 250×250 pixel unless stated otherwise. The

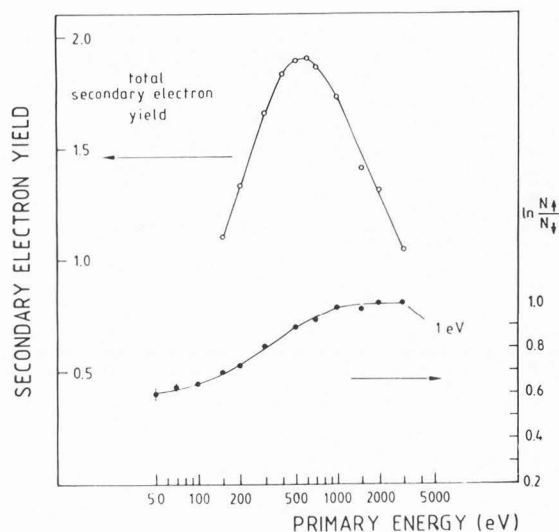


Figure 6. Total secondary electron yield (left-hand scale) and ratio of majority electrons to minority electrons for secondary electrons of 1 eV kinetic energy as a function of the primary electron energy. The polarization P may be obtained from $\ln N_+/N_-$ via the relation $\ln N_+/N_- = \ln[(1+P)/(1-P)] = 2(P+P^3/3+P^5/5+\dots)$.

probe size in all studies except for the high resolution domain wall study, was less than 100 nm. Dwell times per pixel are given in the figure captions if essential.

Single crystal: Fe(100)

Domain images of a Fe(100) single crystal surface are shown in Fig. 7 and Fig. 8. The arrows within the domains indicate their magnetization orientation. A large fraction of the surface ($400 \times 400 \mu\text{m}^2$) is shown in Fig. 7, yielding a survey of the domain pattern. The characteristic structure with domains of highly symmetrical shapes determined by the magnetic properties of iron are to be seen. Fig. 8 shows an interesting detail of the domain pattern, i.e. a magnetic shunt, which is energetically favourable. Similar structures can also be seen in Fig. 7. Both images were taken with the spin analyzer in the 90° bent position (see discussion above), which means that the two measured polarization components are along the surface normal and along one in-plane component of magnetization of the sample. While in the vertical component no polarization was detected, the in-plane component exhibits the structure shown in Fig. 7 and 8. Firstly, this proves the magnetization to lie parallel to the surface, and secondly it demonstrates that in some instances it is sufficient to measure only one in-plane polarization component to obtain the whole magnetization orientation. This works if the magnetic easy axes, i.e. the axes of spontaneous magnetization of the sample, do not coincide with the polarization sensitive axes of the detector. In the case of Fig. 7 and Fig. 8 the polarization sensitive axis is parallel to the vertical picture axes, while the easy axis is tilted by 14°

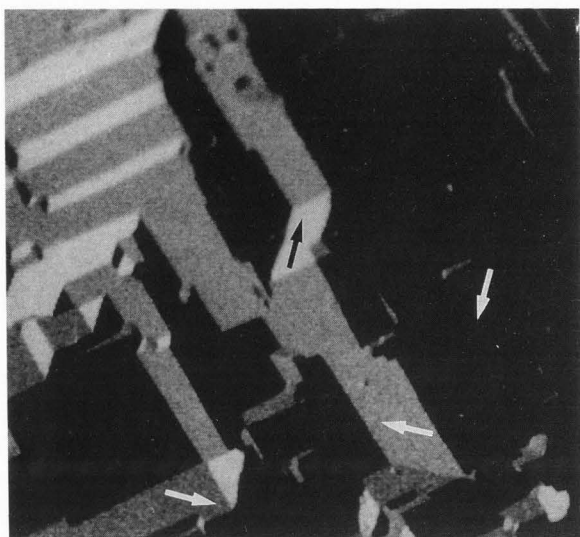


Figure 7. Domain pattern on a Fe(100) single crystal surface. The arrows indicate the magnetization of the domains. The image size is $400 \times 400 \mu\text{m}^2$. The dwell time per pixel was 10 ms.

to the vertical picture axis. As is illustrated in Fig. 9 with this arrangement of detector and sample one obtains four different polarization values due to the different projections of the spontaneous magnetization onto the polarization sensitive direction. The corresponding four different polarization levels are seen in Fig. 10a and b. Fig. 10a and b shows the measured polarization as a function of the position going along a horizontal line slightly above (below) the intersection of the four domains in Fig. 8. The line scans are extracted from the data set of the domain image. For the sake of simplicity the inverted polarization is presented. Each of the constant levels represents one magnetic domain. The highest polarization value belongs to the white, its negative value to the black domain of Fig. 8. The two values around zero represent the light and dark gray regions, respectively. It is apparent from the line scans that the signals from different magnetic areas are well separated and easily distinguishable. For the oppositely magnetized domains (black and white) one can obtain a contrast of > 10 (as estimated above, see discussion about contrast), whereas the contrast between black (or white) and the gray domains is about 5. A low contrast of ~ 2 is obtained between the two gray domains. Nevertheless the two areas are well distinguishable as can be seen in Fig. 7 (lower right corner). The contrast between the gray domains can be increased to > 10 , if both in-plane components are measured (with the detector in the position shown in Fig. 5) with the easy axes coinciding with the two polarization sensitive axes.

Remembering the above discussion and results of the spin-polarized spectroscopy of iron one is led to ask, why the polarization found in the line scans is clearly lower than the value

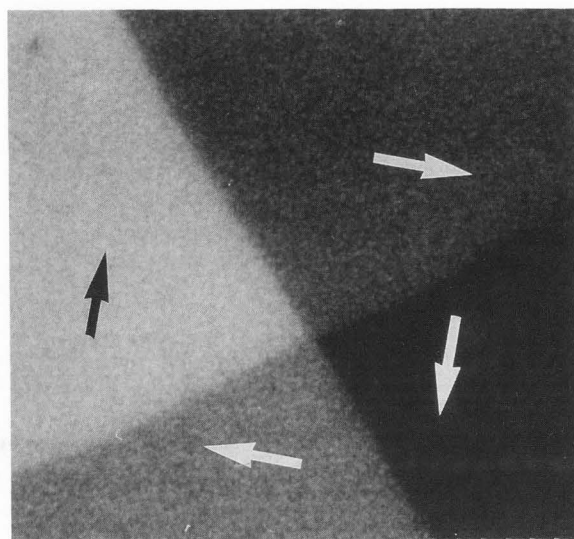


Figure 8. Detail of domain structures in a Fe(100) surface, showing a magnetic shunt. The image size is $33.3 \times 33.3 \mu\text{m}^2$.

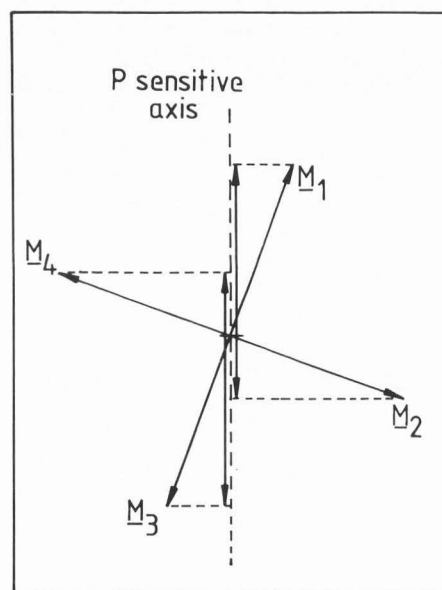


Figure 9. Sketch of the arrangement of easy axes and polarization sensitive directions used for taking the images 7 and 8.

in Fig. 1 of $\lesssim 50\%$. The reason for this reduction is surface contamination by residual gas. From the above considerations about surface cleanliness it is obvious that only a small amount of contamination, e.g. fractions of one monolayer, are sufficient for the reduction found here. If one remembers that at a base pressure of $1 \cdot 10^{-10}$ Torr it takes about 3 hours to cover a clean surface with one monolayer by a residual gas with 100% sticking probability, it is evident that the time for aligning the whole

Imaging of Magnetic Microstructures at Surfaces

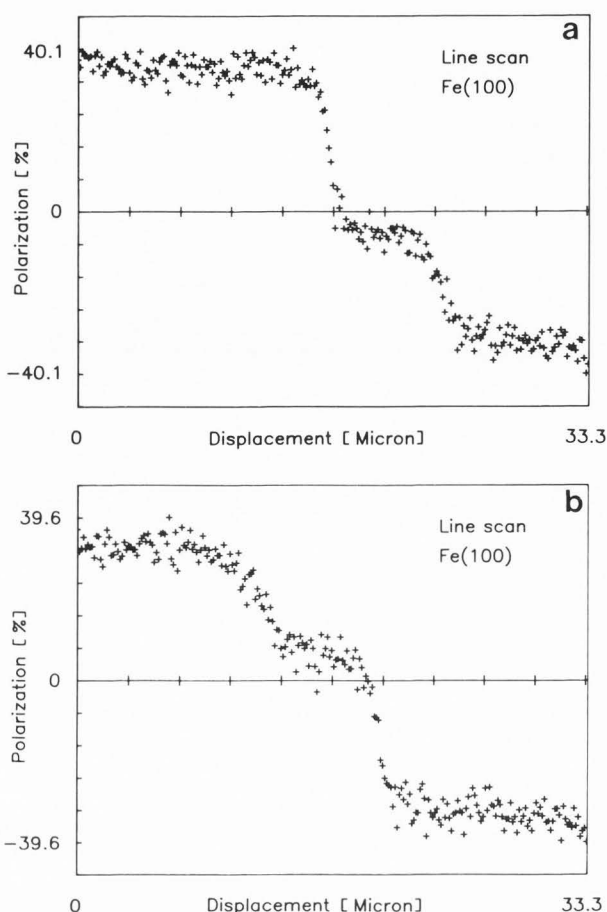


Figure 10. a) Line scan extracted from the data set of Fig. 8 showing the measured polarization distribution along a horizontal line just above the point of intersection of the four domains. For the sake of simplicity the inverted P values are drawn. b) As a) with a line scan extracted from just below the point of intersection.

equipment and searching for interesting structures is sufficient to get a surface coverage that reduces the signal to some extent. However, the results demonstrate, that even in presence of a moderate contamination high-quality pictures may be taken.

Fig. 11 shows the frequency distribution of the measured polarization of Fig. 8 in the form of a histogram. Four peaks are distinguishable representing the four different domains. The separation of the individual peaks again reflects the contrast obtained with the different polarization values, as was discussed with the line scans. The frequency distribution of the polarization is used to set the colour and/or the gray tones for the image. 16 gray levels are normally used for image production. To utilize the whole dynamic range of the gray tone representation an upper and lower bound is set at the right and left footpoint of the distribution (for example at about $\pm 46\%$ in Fig. 11). The

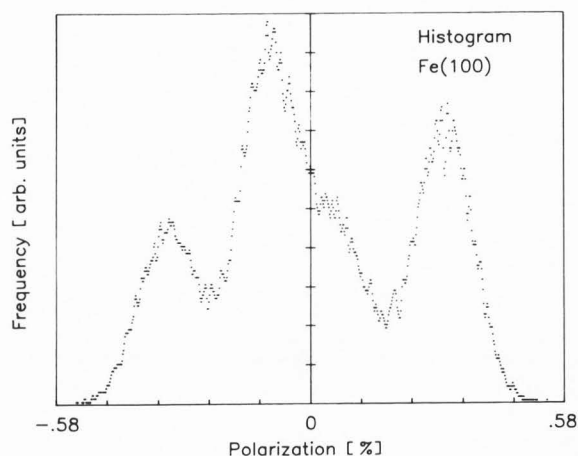


Figure 11. Frequency distribution of the polarization values measured with Fig. 8.

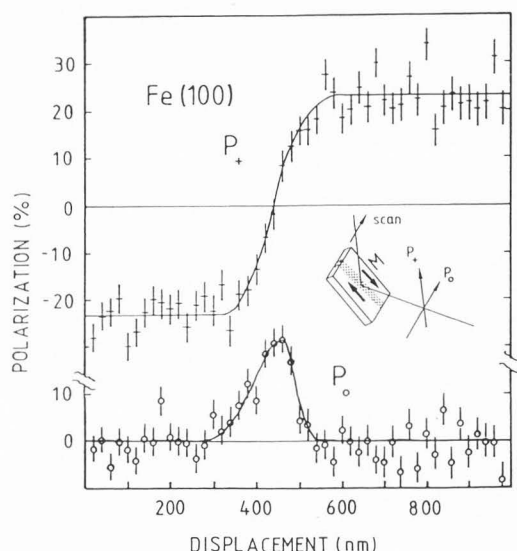


Figure 12. High-resolution line scan across a 180° domain wall at a Fe(100) surface. Inset: The orientation of polarization detection axes relative to the sample. The P_+ component is corrected for the sample tilt. The lines are meant to guide the eye. The step width is 20 nm. The error bars give the 1σ -statistical error.

interval between these two boundaries is divided into 16 equally separated parts, to which the gray levels are appointed. All polarization values within such a subdivision are set to the same gray tone in the image. No further manipulations are necessary to achieve the domain images.

To test the spatial resolution for magnetic structures the smallest structures of the domain pattern have been analyzed, i.e. the domain boundaries. Fig. 12 shows a line scan across a 180° domain wall at the Fe(100) surface. A 180° wall separates two oppositely magnetized domains, e.g. the line where a black and white domain in Fig. 7 intersect. The geometry of the

measurement is seen in the inset of Fig. 12. Both in-plane components of the magnetization were measured, with the polarization sensitive axes aligned with the sample easy axes. One component ("+") is parallel to the domain magnetization and thus reflects the change in magnetization (respectively polarization) while crossing the domain wall. The transition appears to be continuous, indicating that the magnetization turns around within the wall as $|M(r)| = \text{const}$ within a homogeneous magnet. The second in-plane component ("o") shows how the magnetization vector turns around inside the wall. Within the domains this component exhibits no spin polarization; in the transition region, however, the polarization raises to its maximum value. Thus it is obvious that the magnetization vector turns around totally within the surface plane. This domain wall structure is commonly known as a Néel wall. Since in the bulk the wall is of Bloch-like structure, the termination into a Néel-like structure at the surface is a consequence of the very existence of the surface itself (Oepen and Kirschner, 1989; Scheinfein et al., 1989).

Let us turn back to the question of the attainable resolution for magnetic structures. From the line scan studies (Fig. 12) we can estimate an upper limit for the achievable resolution. The step width, e.g. the spacing between adjacent points, is 20 nm. Looking at the right edge of the bump in the "o" component one can see a drop of the polarization from nearly maximum to nearly zero within two measuring points. From that we deduce a resolution of ≤ 40 nm for an iron sample as an upper limit. As such a domain wall exhibits a continuous change of the signal it is hard to demonstrate the resolution in the conventional sense of microscopy with a domain image of Fe(100). The achievable resolution in domain images is of the same order of magnitude, although this is not generally valid as it depends on the contrast that is attainable in reasonable times and thus it depends strongly on the magnetic properties of the material.

Ultrathin films: Co/Cu(100)

The high surface sensitivity of the technique is very advantageous for the study of magnetic structures in ultrathin films. Co films in the thickness range of a few monolayers were epitaxially grown on a Cu(100) single crystal surface. They grow in a fcc modification. Both the preparation of the substrate surface as well as the evaporation of the films were done *in situ* to achieve perfect films with absolutely clean surfaces. The domain image from a 5.5 monolayer thick cobalt film is shown in Fig. 13. The arrows indicate the magnetization orientation of the domains. The easy axes were found to be parallel to the {110} directions and within the film plane. Domains of all four possible magnetization orientations are seen in Fig. 13. Some small disturbances (lower left corner) can be identified, which do not affect the large gray domain, whereas the domain wall between the white and the black domain is pinned by such a disturbance.

We have tested the thickness dependence of the signal (polarization) with the measurements on the ultrathin films. Fig. 14 shows a plot of the spin polarization normalized to its value for thick films vs the thickness. An independent quantity for comparison is the intensity of hysteresis loop measurements taken with the magneto-optical Kerr effect. The Kerr intensities are divided by the film thickness to eliminate the linear dependence of the Kerr ellipticity on film thickness (Moog et al., 1989). The Kerr effect data were then fitted to the polarization measurement data in the overlapping thickness range. From Fig. 14 it is obvious that both sets of data exhibit the same tendency of the thickness dependence of the signal. As both techniques yield quantities which are proportional to the saturation magnetization we may interpret this result to reflect the thickness dependence of the saturation magnetization M_S , well known from studies of thin film magnetism (Gradmann, 1974). At a thickness of three monolayers, however, there is a striking deviation of the two sets of data. The polarization values are lower than the Kerr data. Below 3 monolayers the deviation becomes stronger and the polarization signal rapidly vanishes. This behaviour is caused by the decrease of the polarization due to an increasing amount of unpolarized secondary electrons from the copper substrate. This indicates the escape depth of the secondary electrons to become comparable with the film thickness. Thus the spin polarization is no longer proportional to the magnetization below 3 monolayers. We may conclude from this result that the magnetic depth of information is about 3 monolayers, which is in excellent agreement with the values mentioned above.

Fig. 14 demonstrates the necessity of a highly surface sensitive technique to study the micromagnetic structures in ultrathin films, as the magnetization drops drastically with decreasing film thickness. Fig. 15 and Fig. 16 demonstrate the feasibility of domain observation in very thin films with the scanning microscope with spin polarization analysis. The film thickness is 3.5 monolayers and 3 monolayers, respectively. To obtain these images a measuring time of 30 msec/pixel was taken. For the oppositely magnetized domains in Fig. 15 (black and white) the contrast is still high. In Fig. 16 the contrast is lower but still sufficient to obtain detailed microstructures, although the magnetization in the domains differ only by 90° , which generally yields a lower contrast (see discussion about contrast). Fig. 15 and Fig. 16 exhibit some of the characteristic features found in our studies of ultrathin films. Firstly the domain walls are very irregular compared with the results for bulk iron (see Fig. 7 and Fig. 8). Secondly, the domain wall width varies depending on their relative orientation with respect to the magnetization orientation of the adjacent domains (see Fig. 15). The studies of ultrathin films are still under progress. For more details the reader is referred to Oepen et al. (Oepen et al., 1990).

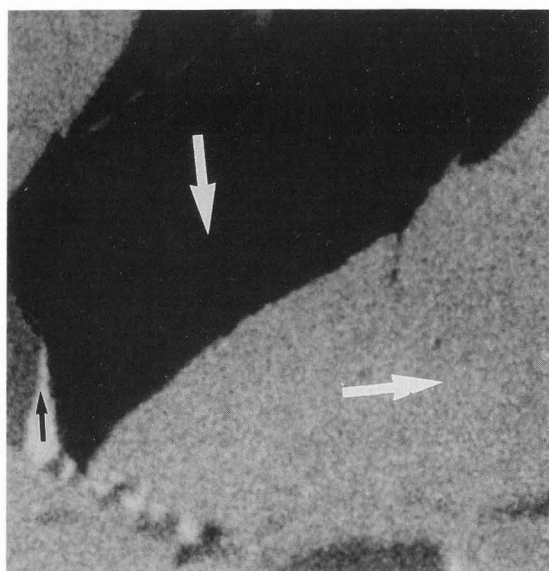


Figure 13. Domain image of a 5.5 monolayer thick cobalt film on Cu(100). The image size is $100 \times 100 \mu\text{m}^2$.

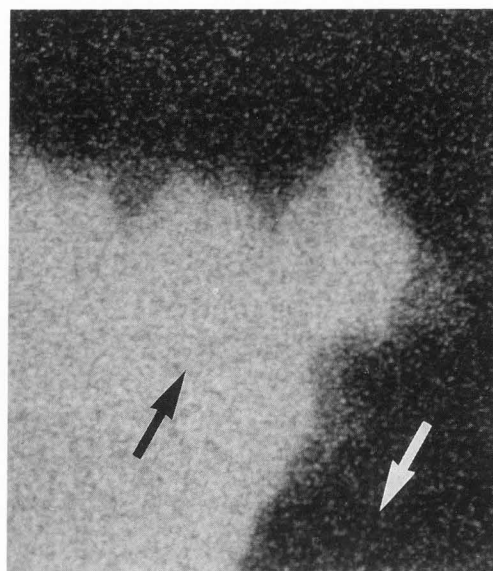


Figure 15. Domain image in a 3.5 monolayer thick cobalt film on Cu(100). The picture size is $25 \times 25 \mu\text{m}^2$.

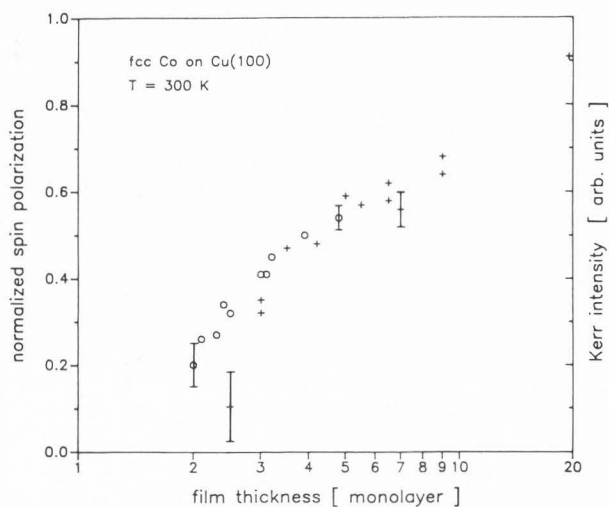


Figure 14. Normalized spin polarization vs Co film thickness. The spin polarization values taken from the domain structure investigation (+) are normalized to the value of thick cobalt films. The data are combined with magneto-optical Kerr effect measurements (o). The Kerr data are normalized with respect to the film thickness and fitted to the polarization data in the region of 3.5-5 monolayers. The two techniques were performed in different laboratories, completely independently of each other.

Video tape: $\text{Co}_{80}\text{Ni}_{20}$

Recorded tracks in a $\text{Co}_{80}\text{Ni}_{20}$ video tape are seen in Fig. 17. The recording medium is evaporated onto an aluminum coated PET polymer. The thickness is about 150 nm. The recording was

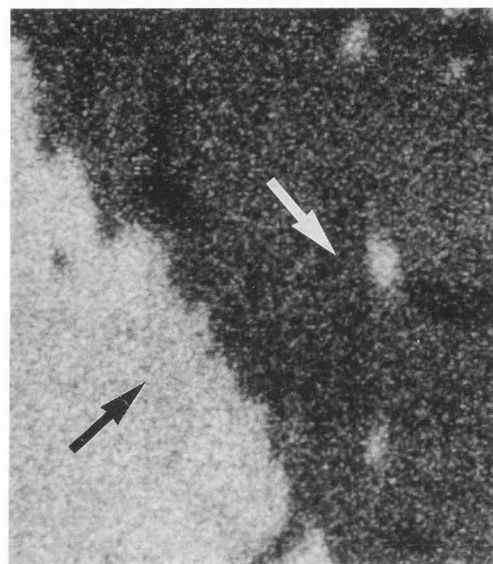


Figure 16. Domain image in a 3 monolayer thick cobalt film on Cu(100). The image size is $50 \times 50 \mu\text{m}^2$.

done at a constant frequency, yielding an average domain width of $\sim 4.3 \mu\text{m}$. Due to the writing process of the video recording unit the domains in adjacent tracks are tilted by 15° . The tape transport direction is nearly parallel to the vertical picture edge. Two different writing heads are used to record a pair of tracks separated by $5 \mu\text{m}$. The next track pair is written $10 \mu\text{m}$ away. Due to the production process the easy axis is parallel to the transport direction. Deviations from that direction were found for the

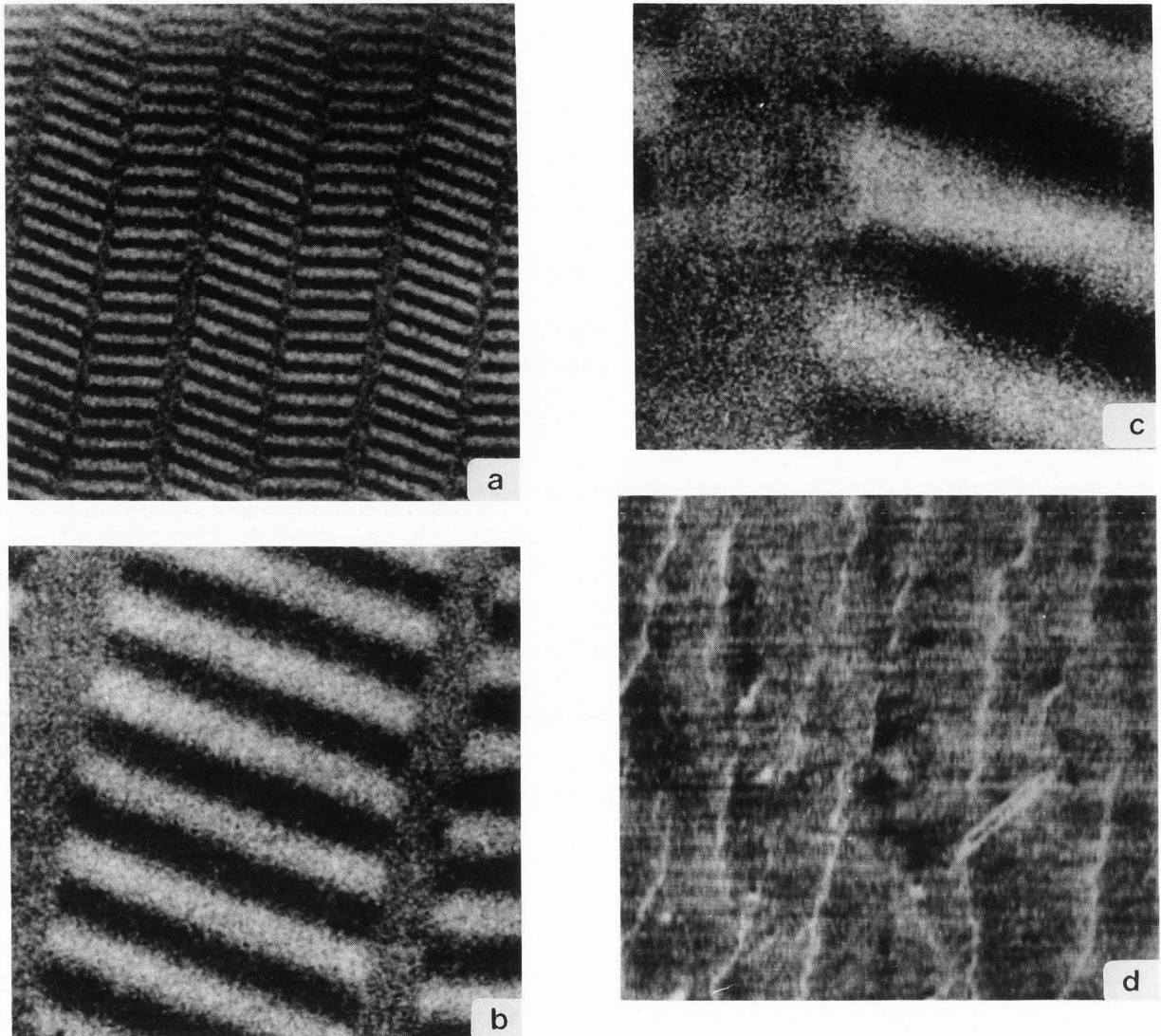


Figure 17. Recorded tracks in a $\text{Co}_{80}\text{Ni}_{20}$ video tape. a) Image size of $200 \times 200 \mu\text{m}^2$, b) Enlarged section from a). Size $50 \times 50 \mu\text{m}^2$, c) Enlarged section from b). Size: height $22 \mu\text{m}$, width $25 \mu\text{m}$; 220×250 pixel, d) Topographic image of Fig. 17b, obtained from the same set of data as Fig. 17b. The topographic image results from the sum of the diffraction beam intensities.

magnetization of the domains in the tracks tilted against the transport direction. The magnetization orientation was parallel to the track direction, thus a tilt of $\sim 15^\circ$ to the easy axes exist. The other tracks exhibit domains magnetized nearly parallel to the easy axis. No magnetization component perpendicular to the tape was found. Those data confirmed suggestions from Lorentz microscopy studies (Ferrier et al., 1987) about the magnetization orientation in the tracks written with different heads. The transition region between the domains are by no means sharp as one can see with the higher magnification in Fig. 17b and 17c. Moreover the domain

width varies across the tracks, which means that the writing yields no well-defined domains. These findings will effect the smallest size of stored domains, respectively the attainable storage density. At the edge of the tracks the domains deviate strongly from the ideal bar size. This is caused by the writing as the heads write only over a distance of approximately $17 \mu\text{m}$ in the track centre. In Fig. 17c some weak crosstalk, i.e. a coupling of domain structures of adjacent tracks via a magnetization of the material in between, is visible.

Fig. 17d is the topographical image taken simultaneously with the domain image of Fig. 17b. It is obtained from the sum of the count rates used to measure the asymmetry. Cracks in the evaporated storage material as well as some particles on the surface can be seen. Intensity fluctuations yield horizontal stripes in the image. This is due to a high frequency flickering of the field emission source. Nothing of this real and noise-induced structure of the intensity image is seen in the magnetic domain image.

This demonstrates that topographical as well as intensity fluctuations are eliminated due to the normalization in the asymmetry formula.

Vertical recording medium: Co₇₉Cr₂₁

Polycrystalline CoCr thin films with vertical magnetization are promising candidates for ultrahigh density storage media (Iwasaki, 1984), as the transition regions between oppositely magnetized domains are very narrow. The thin CoCr films exhibit a columnar structure. The columnar grains show an hcp crystal structure with the c-axis normal to the films. This special feature is responsible for a high uniaxial anisotropy perpendicular to the film, which means that the spontaneous magnetization tends to align with the film normal direction. Such a desired alignment can be suppressed by the demagnetizing field, which can turn the magnetization into the film plane, if the saturation magnetization is high. To achieve a high uniaxial anisotropy as well as a low saturation magnetization a certain amount of chromium is necessary. For storage media purposes a chromium concentration of 18-24% has been recommended in the literature.

A recorded track in such a new storage medium is to be seen in Fig. 18a,b. The film has a thickness of 400 nm and is exactly the same as used for actual data storage devices, but without the protective layer. The two images (Fig. 18a,b) show the domain pattern obtained with the in-plane component of magnetization (parallel to the vertical picture axis) in Fig. 18a and with the vertical magnetization component (Fig. 18b). Due to the low saturation magnetization (and thus polarization signal) the contrast is very weak. The vector sum of both components yields about one tenth of the signal found with iron. As mentioned above (see discussion about contrast) the contrast that can be achieved with such samples is strongly limited by the low polarization signal. Nevertheless the images demonstrate the feasibility of imaging magnetic domain structures even in such a worst case situation. Moreover, our investigation yields new insight into the magnetic properties of this material as will be discussed in the following.

Comparing both images it is obvious that the in-plane component exhibits a better contrast than the vertical one, indicating that the in-plane signal is higher. This conjecture is confirmed by the analysis of the measured polarization values, from which a tilt of the magnetization vector against the film plane of about 30° can be deduced. This finding is very surprising in the light of the above considerations on the properties of such material. As our technique is surface sensitive, that finding has to be attributed to the surface properties. It demonstrates that at the surface, in spite of the strong vertical anisotropy and low saturation magnetization, the magnetization has the tendency to form closure structures. This should affect the stray fields above the surface and thus the reading process. One could also think of an influence on the achievable storage density.

The investigation of the CoCr storage medi-

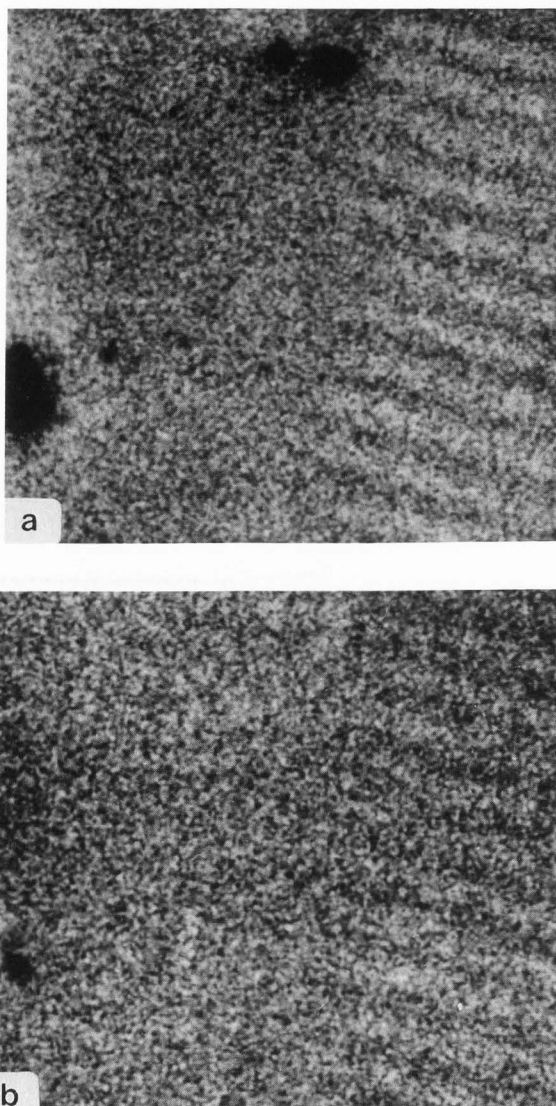


Figure 18. Recorded track in a CoCr storage medium. The image size is $20 \times 20 \mu\text{m}^2$. The dwell time per pixel was 30 ms. a) Domain structure obtained with the in-plane component of magnetization. b) Domain structure obtained with the vertical component of magnetization.

um is another important proof for the necessity of measuring directly the magnetic properties, i.e. the magnetization orientation. Several other techniques have been used for studying domain structures in CoCr storage media, such as Kerr-microscopy (Schmidt and Hubert, 1986) Bitter-technique (Iwasaki et al., 1980) as well as magnetic force microscopy (Grütter et al., 1989), but no deviation from a vertical magnetization orientation was observed. This is mainly due to the techniques used, measuring secondary effects, related to the magnetization, but not proportional to it.

Conclusion

In this paper the advantages and limitations of scanning electron microscopy with spin polarization analysis have been discussed. Many more examples of features of this type of microscope can be found in papers on special topics in the literature. Clearly there are limitations of the technique, but its advantages prevail. The development of several other microscopes of this type is the best indication for its capabilities. In many applications the spin polarization provides the essential information on magnetic properties not available with other domain imaging techniques. The high spatial resolution and the capability of studying semi-infinite samples bear its relevance for the application in the study of new storage media. The capability of studying ultrathin films will gain more and more importance for basic research and technological developments in the near future.

Acknowledgement

We wish to acknowledge the collaboration of C.M. Schneider and P. Bressler (Freie Universität Berlin) and M. Benning (IGV/Jülich) for their help and support in the production of the ultrathin films. Helpful discussions with Professor H. Ibach are gratefully acknowledged. Special thanks go to A. Berger for his assistance with the iron measurements and to J. Larscheid and K. Hieble for their technical assistance. We wish to thank Siemens Research Laboratories, Erlangen, for the CoCr storage medium.

References

Abraham DL, Hopster H (1987) Magnetic probing depth in spin-polarized secondary-electron spectroscopy. *Phys. Rev. Lett.* **58**, 1352-1354.
 Allenspach R, Taborelli M, Landolt M (1985) Oxygen on Fe(100): An initial-oxidation study by spin-polarized Auger spectroscopy. *Phys. Rev. Lett.* **55**, 2599-2602.
 Bitter F (1931) On inhomogeneities in the magnetization of ferromagnetic materials. *Phys. Rev.* **38**, 1903-1908.
 Chapman JN, Morrison GR (1983) Quantitative determination of magnetization distributions in domains and domain walls by scanning transmission electron microscopy. *J. Mag. Mag. Mat.* **35**, 254-260.
 Chobrok G, Hofmann M (1976) Electron spin polarization of secondary electrons ejected from magnetized europium oxide. *Phys. Lett.* **57A**, 257-258.
 DiStefano TH (1978) Technology for detecting small magnetic domains and beam-addressed memory therewith. *IBM Tech. Disc. Bull.* **20**, 4212-4215.
 Ferrier RP, Ferry MD, Wales JLS (1987) Studies of the micromagnetic structure of recorded tracks in MET. *JEEE Trans. Magn. Mag-22*, 3639-3641.
 Gradmann U (1974) Ferromagnetism near surfaces and in thin films. *Appl. Phys.* **3**, 161-178.
 Grütter P, Wadas A, Meyer E, Hidber H-R,

Güntherodt H-J (1989) Magnetic force microscopy of a CoCr thin film. *J. Appl. Phys.* **66**, 6001-6006.
 Hámos LV, Thiessen PA (1931) Über die Sichtbarmachung von Bezirken verschiedenen ferromagnetischen Zustandes fester Körper. (Visualization of domains of different ferromagnetic states in solids.) *Z. Phys.* **71**, 442-444.
 Iwasaki S, Ouchi K, Honda K (1980) Studies of the perpendicular magnetization mode in Co-Cr sputtered films. *JEEE Trans. Magn. Mag-16*, 1111-1113.
 Iwasaki S (1984) Perpendicular magnetic recording - evolution and future-. *JEEE Trans. Magn. Mag-20*, 657-662.
 Jacobovics JP (1973) Lorentz Microscopy and applications (TEM and SEM). In: *Electron Microscopy in Materials Science IV*, Ruedl E and Valdré U (eds.), Commission of the European Communities, Brussels, 1305-1403.
 Kessler J (1985) *Polarized Electrons*, Springer Verlag, Berlin, 230-244.
 Kirschner J (1984) On the role of the electron spin in scanning electron microscopy. *Scanning Electron Microsc.* **1984**; **III**: 1179-1185.
 Kirschner J (1985) *Polarized Electrons at Surfaces*. Springer Verlag, Berlin, 61-71.
 Kirschner J, Suga S (1987) Spin polarization vector analysis of secondary electrons from ferromagnetic Fe excited by spin-polarized primary electrons. *Solid State Commun.* **64**, 997-1000.
 Kirschner J, Koike K, Oepen HP (1988) Spin polarization of ion-excited secondary electrons from ferromagnets and its application for magnetic sputter profiling. *Phys. Rev. Lett.* **59**, 2099-2102.
 Kirschner J (1988) Spin-polarized secondary electrons from ferromagnets. in: *Surface and interface characterization by electron optical methods*, Howie A and Valdré U (eds.), Plenum Publishing Corporation, 267-283.
 Kisker E, Gudat W, Schröder K (1982) Observation of high spin polarization of secondary electrons from single crystal Fe and Co. *Solid State Commun.* **44**, 591-595.
 Koike K, Hayakawa K (1984a) Scanning electron microscope observation of magnetic domains using spin-polarized secondary electrons. *Jpn. J. Appl. Phys.* **23**, L187-L188.
 Koike K, Hayakawa K (1984b) Observation of magnetic domains with spin-polarized secondary electrons. *Appl. Phys. Lett.* **45**, 585-586.
 Koike K, Matsuyama H, Hayakawa K (1987) Spin-polarized scanning microscopy for micro-magnetic structure observation. *Scanning Microsc.* **1987**; **I**: 241-253.
 Koike K, Matsuyama H, Hayakawa K (1988) Spin-polarized scanning electron microscope equipped with a thumb-size spin detector. *Jpn. J. Appl. Phys.* **27**, L1352-L1354.
 Levi-Setti R, Chabala J, Wang YL (1987) Micro-secondary ion mass spectroscopy: Physical and instrumental factors affecting image resolution. *Scanning Microsc.* **1**, 13-22.
 Makharov VV, Petrov NN (1981) Regularities of secondary electron emission of elements of the periodic table. *Sov. Phys. Solid State* **23**, 1028-1032.

Moog ER, Zak J, Hubermann ML, Bader SD (1989) Magneto-optic rotation and ellipticity of ultrathin ferromagnetic films. *Phys. Rev.* **B39**, 9496-9499.

Newbury DE, Jon DE, Echlin P, Fiori CE, Goldstein JI (1986) *Advanced Scanning Electron Microscopy and X-ray Microanalysis*. Plenum Press, New York, 147-179.

Open HP, Kirschner J (1988) Imaging of magnetic microstructures at surfaces. *Journal de Physique Coloque C8, Supplement au No 12, tome 49*, 1853-1857.

Open HP, Kirschner J (1989) Magnetization distribution of 180° domain walls at Fe(100) single-crystal surfaces. *Phys. Rev. Lett.* **62**, 819-822.

Open HP, Benning M, Ibach H, Schneider CM, Kirschner J (1990) Magnetic domain structure in ultrathin cobalt films. *J. Magn. Magn. Mater.* **86**, L137-L142.

Rave W, Schäfer R, Hubert A (1987) Quantitative observation of magnetic domains with the magneto-optical Kerr effect. *J. Mag. Magn. Mat.* **65**, 7-14.

Scheinfein MR, Unguris J, Celotta RJ, Pierce DT (1989) Influence of the surface on magnetic domain-wall microstructure. *Phys. Rev. Lett.* **63**, 668-671.

Schmidt F, Hubert A (1986) Domain observations on CoCr-layers with a digitally enhanced Kerr-microscope. *J. Mag. Mat.* **61**, 307-320.

Schneider CM, Bressler P, Schuster P, Kirschner J, de Miguel JJ, Miranda R (1990) Curie temperature of ultrathin films of fcc cobalt epitaxially grown on atomically flat Cu(100) surfaces. *Phys. Rev. Lett.* **64**, 1059-1062.

Seiler H (1983) Secondary electron emission in the scanning electron microscope. *J. Appl. Phys.* **54**, R1-R18.

Siegmann HC, Pierce DT, Celotta RJ (1981) Spin-dependent absorption of electrons in a ferromagnetic metal. *Phys. Rev. Lett.* **46**, 452-455.

Tomomura A (1983) Observation of magnetic domain structure in thin ferromagnetic films by electron holography. *J. Mag. Mag. Mat.* **31-34**, 963-969.

Unguris J, Pierce DT, Galejs A, Celotta RJ (1982) Spin and energy analyzed secondary electron emission from a ferromagnet. *Phys. Rev. Lett.* **49**, 72-76.

Unguris J, Hembrel G, Celotta RJ, Pierce DT (1985) High resolution magnetic microstructure imaging using secondary electron spin polarization analysis in a scanning electron microscope. *J. Microscopy* **139**, RP1-RP2.

Unguris J, Pierce DT, Celotta RJ (1986) Low-energy diffuse scattering electron-spin polarization analyzer. *Rev. Sci. Instrum.* **57**, 1314-1323.

VanZandt V, Browning R, Helms CR, Poppa H, Landolt M (1989) A novel approach to image processing in spin-polarized electron microscopy. *Rev. Sci. Instrum.* **60**, 3430-3433.

Discussion with Reviewers

J. Unguris: It is not obvious without doing the necessary convolutions of analyzer response with secondary electron polarization and intensity

energy dependence what the optimal energy acceptance is. Was the 0 to 6 eV analyzer window selected in this manner? If not, what is the optimal energy window?

Authors: We did not do a convolution of analyzer response with the distribution of polarization and intensity of the secondary electrons, as both distributions are not well enough known for the geometry and extraction voltage used. We have performed some experimental checks however: An increase of the pass energy by a factor of 1.5 (i.e. $\Delta E = 9$ eV) gives a small increase in intensity (15 %), while the measured polarization drops. A decrease in the energy window, on the other hand, causes a strong decrease in intensity while the polarization slightly increases. As we checked this in steps of 1 eV only, the P²I value might be slightly higher anywhere around 6 eV. The setting we use, however, is very close to the optimum for our analyzer including its electron optics.

R. Allenspach: You give a short discussion on possible influence of stray magnetic fields (of the column) on measured spin direction due to spin precession. In that respect it would be nice to have some numbers concerning the stray field at the sample, and maybe some estimate why this influence is so small.

Authors: Calculations of the spin-rotation in the stray magnetic field of the column give a spin precession of less than 5° in our configuration. Some of the parameters taken for the calculation are: i) Working distance: 10 mm ii) $E_p = 5$ KeV iii) Stray magnetic field $B = 2,66 \cdot 10^{-4}$ T at the sample iv) Accelerating of the SE into the electron optics within a field of 50 V/mm v) Worst case: P_{IB} always and $B = \text{const}$, i.e. equal to the stray field at the sample.

K. Koike: In Fig. 17 and 18, you show the recorded pattern on magnetic storage media of both in-surface-plane and perpendicular recording. These samples have relatively large leakage magnetic field near the sample surface. The field would influence the image contrast in two ways, i.e., rotation of secondary electron spin and deflection of secondary electron trajectory which would result in a scattering asymmetry in a polarization detector. Have you estimated these effects for the analysis of magnetization distribution?

Authors: We have made some worst case calculations for the spin precession as well as for deflection due to the Lorentz force. For CoCr we obtain a spin rotation of less than 5°, with $M_S = 1/4 M_S(\text{Fe})$ and for CoNi we calculated this angle to be $< 8^\circ$ ($M_S = 1/2,75 M_S(\text{Fe})$). For the calculation we took P_{IB} always with the magnetic field of a periodic structure and the magnetic field of a charged line. Due to the periodicity, or the small width of the line respectively, the field drops strongly with increasing distance from the surface and the influence of the sample stray field on the secondary electron polarization is very small.

The deflection of the electrons by the Lorentz force is negligibly small. For CoCr the

2 eV electrons are deflected in the field of the storage medium by less than 1° . For the video tape the results themselves answer the question. As the measured polarization within a written bit is constant, one may deduce that the varying B field above the bit does not influence the asymmetry drastically. Thus this effect is of minor importance and not detectable within our error margin.

J.N. Chapman: Secondary electrons are created by back-scattered electrons as well as by primaries. What effect do they have? Do they just add to the noise and, if so, how are the formulae 13 realistically affected?

Authors: The SE_{II} are of minor importance for the domain structure and the obtained contrast as long as the domain size is large compared to the emission region of the SE_{II} (e.g. for $E_p = 10$ KV the size of this area is about μm). The SE_{II} do not effect the signal nor the noise in that case as they have the same polarization. The resolution, however, may be altered by them and one has to take backscattered electrons into account in high resolution studies. One point to overcome this problem (e.g. in domain wall investigation) is to lower the primary electron energy (the lower the better).

J.N. Chapman: Fig. 12: Why does $P_o(\max)$ not equal 25, as does $P_+(\max)$? I think hard magnetic materials are best for a resolution test. Do the authors agree?

Authors: We think that, within the error margin, $P_o(\max)$ is the same as $P_+(\max)$. Please note the fluctuation in "+" as well. The line in "+" is meant to guide the eye. You are right with the hard magnetic material. One appropriate candidate for that would be the prism plane of a Co single crystal.

R. Allenspach: What determines finally the resolution in magnetic imaging? How is resolution in magnetic imaging defined reasonably? If it is taken as a 10 to 90 % transition width as sometimes done for intensity, one arrives at 50 nm from the "o" component in Fig. 12.

Authors: The main question concerning the lateral resolution is not whether one takes 10-90 % or any other value, but the problem is again the contrast, i.e. the signal-to-noise-ratio as compared to the time necessary to obtain a good contrast. With samples that give low signal (small P), it is hardly possible to achieve high contrast in reasonable times, which means that due to the high noise level (with respect to the signal) fine structures are invisible. An interesting paper by Levi-Setti et al. (Levi-Setti et al., 1987) is dealing with this subject, although it is applied to SIMS.

J. Unguris: In the CoCr thin film measurements, why is the polarization only one tenth that of Fe?

Authors: We have also been surprised by this low polarization value. To our opinion, however, that finding might not be too surprising if one takes segregation effects into consideration. If the composition in the few top most layers is changed due to segregation of one species to the

surface, this should alter the magnetic properties. A chromium segregation for example could cause a reduction of M_s as with a higher chromium concentration the composition may come near to the compensation point. Such a composition gradient in the first few layers cannot be resolved by Auger spectroscopy. Thus, although approximately the nominal Auger composition was found (and no differential sputtering effects were found) the surface composition in the top layer(s) might be sufficiently different to affect the surface magnetic properties.

Also, the 'rule of thumb' of the polarization scaling with the saturation magnetization might not hold in this case. This 'rule' has so far a purely experimental basis only and has not been checked in cases of very low saturation magnetization.

J.N. Chapman: I would find a schematic of what the authors think is the magnetization distribution in CoCr useful.

Authors: We are sorry about the missing explanation and we cannot give any. Firstly, we did not get enough information about the material properties from our supplier. Secondly, the industrial company is not interested in seeing these details published. The only reliable information we have, is that exactly the same material has been used for prototype storage media.

R. Allenspach: For the non-expert in the field it would be nice to have some relevant parameters to judge the easiness or difficulty of the experiment. This holds in particular for Fig. 18 where the polarization values would be interesting since this image seems to show the present limit of the technique.

Authors: The measured polarization values are (i) For the in-plane component (Fig. 18a) $P \approx \pm 3.2\%$, i.e. a scattering asymmetry of $A \approx \pm 0.8\%$. (ii) For the vertical component (Fig. 18b) $P \approx \pm 1.6\%$ ($A \approx \pm 0.4\%$).

O.C. Wells: I would like to see some discussion of signal-to-noise ratio. It would seem that the signal conversion efficiency of the detector is not very good. Is this a fundamental limit, or is there hope to improve on this? In the ordinary SEM it is hard enough to get good spatial resolution even with a highly efficient detector of the secondary electrons, and it must be much more difficult here. For time-resolved studies, the beam must be pulsed with a small duty cycle to follow rapid changes in the specimen. How would this affect the spatial resolution here?

Authors: The sensitivity of the polarization detection is one great limitation of the technique. For all existing detectors the figure of merit is of the order of 10^{-4} while it could, in principle, be of order 10^{-1} . Unfortunately, nobody has yet invented such a device, which would greatly improve the performance of this type of microscopy.